Hydrogen Purification

DOI: 10.1002/anie.201005650

High Catalytic Performance of Ruthenium-Doped Mesoporous Nickel–Aluminum Oxides for Selective CO Methanation**

*Aihua Chen, Toshihiro Miyao, Kazutoshi Higashiyama, Hisao Yamashita, and Masahiro Watanabe**

As fuel-cell research and development has become a flourishing area in recent years, fuel processing, including hydrogen generation, purification, and storage is drawing a great deal of attention. At present, most hydrogen is synthesized through the steam reforming of hydrocarbon fuels, and the water-gas shift of CO (WGS) inevitably coproduces 0.5–1 vol% of CO. However, the polymer electrolyte fuel cell (PEFC) is poisoned easily if the CO concentration is higher than 10 ppm.[1–4] Preferential oxidation of CO (PROX) has been proposed as a "deep-cleaning" process: CO is oxidized to CO_2 with air supplied downstream from the WGS reactor; it has succeeded in meeting the requirements of the PEFC.[5–10] However, this process requires an external air supplier, a cooling system, and a mixer for reformate gas and air, which makes it necessary to explore other more cost-effective approaches. The process of CO methanation, that is, direct hydrogenation of CO to methane and water by consumption of three moles of hydrogen, has been investigated as a less costly, space-saving substitute for PROX that requires no additional reactants.[11–18] Moreover, the CH_4 produced by this reaction can be reused by recirculating the anode off-gas into the reformer as a combustion fuel for reforming. However, to date, there is still a major challenge to remove 1 vol% CO down to lower than 10 ppm under standard operating conditions. Furthermore, maintaining the selectivity of CO methanation is another challenge owing to the presence of about 20 vol% of CO_2 in reformate hydrogen fuels, which will also generate methane by consuming four moles of hydrogen at relatively high temperatures, and which is often accompanied by another side reaction, the reverse water-gas-shift (RWGS) reaction by converting CO_2 into CO. The exothermic character of both methanation reactions also causes problems with the exact control of the reaction temperature, which can result in a further increase in conversion of CO_2. For the sake of maintaining selectivity, the reaction temperature should be controlled to be as low as possible; specifically, lower than 250 °C. Moreover, the equilibrium temperature for the WGS reactor in the case of 1 vol% residual CO is around 230 °C. Considering practical applications, the most suitable temperature range for CO methanation is 200–250 °C. Furthermore, the long-term stability of the catalyst is another important factor. Consequently, for the effective removal of CO by means of catalytic methanation, the following three requirements should be met: 1) high performance, including activity and selectivity; 2) a wide working temperature window, including the range of 200–250 °C; and 3) good stability.

Nickel- and ruthenium-based catalysts have been reported to be the most effective ones for selective CO methanation by Takenaka et al.[19] They reported that Ni/ZrO_2 and Ru/TiO_2 showed the highest catalytic activities among a series of catalysts studied for this reaction, reducing CO levels from 0.5 vol% to 20 ppm, accompanied by low CO_2 conversion in the presence of 25 vol% CO_2, but in a narrow reaction temperature range. Such catalytic performance has been related to the size and shape of the metal nanoparticles and the interactions between the metals and the oxide supports.[20] Recently, we reported superior selective CO methanation with H_2 in reforming gas on Ni-Al mixed oxides modified by 1 wt% Ru (surface area 130 $m^2 g^{-1}$) synthesized by a solution-spray plasma technique.[21] The best catalyst can decrease CO levels from 1 vol% to 13 ppm at about 210 °C with a reaction selectivity of 80%. We concluded that ruthenium plays an important role, not only enhancing the formation of CO methanation active sites of nanosized nickel particles formed on the surface of $NiAl_2O_4$ by reduction with spill-over hydrogen, but also improving the selectivity by the suppression of CO_2 dissociation over nickel metal sites. Herein, we demonstrate for the first time that mesoporous Ni-Al oxides with high surface areas synthesized by the sol–gel method, doped with a small amount of ruthenium through a conventional impregnation process, successfully avoid the formation of $NiAl_2O_4$ and show excellent catalytic performance for selective CO methanation.

A series of mesoporous Ni-Al oxides, denoted as MA-*x*Ni (*x* is defined as the nickel mole percent relative to Ni plus Al; $100 \times Ni/(Ni+Al)$), was prepared by a sol–gel method using evaporation-induced self-assembly, following the method proposed by Morris et al.[22] Wide-angle X-ray diffraction (XRD) patterns of the powder indicate the amorphous nature of MA-*x*Ni ($x = 0$, 10, and 20) calcined at 400 °C. When $x = 33$, broad peaks assigned to NiO are observed, which become sharper at higher nickel fractions (Supporting Information, Figure S1). The presence of uniform, hexagonally ordered mesopores for the samples up to 20% Ni was confirmed by TEM analysis (Supporting Information, Figure S2). The

[*] Dr. A. Chen, Prof. T. Miyao, Prof. K. Higashiyama, Prof. H. Yamashita, Prof. M. Watanabe
Fuel Cell Nanomaterials Center, University of Yamanashi
6-43 Miyamae-cho, Kofu, Yamanashi 400-0021 (Japan)
Fax: (+81) 55-254-7091
E-mail: m-watanabe@yamanashi.ac.jp
Homepage: http://fc-nano.yamanashi.ac.jp

[**] This research was financially supported by the New Energy and Industrial Technology Development Organization (NEDO) of Japan.

Supporting information for this article is available on the WWW under http://dx.doi.org/10.1002/anie.201005650.

EDAX mapping images prove the uniform dispersion of Ni and Al in the mesopore skeleton. The ordered mesoporous structure was maintained when a small portion of Al in the hexagonal mesoporous skeleton was replaced by Ni, but this structure was disrupted with further increases in Ni mole fraction (Supporting Information, Figure S2). High BET surface areas (ca. 350 $m^2 g^{-1}$) of mesoporous MA-*x*Ni were obtained at $x < 33$, but the areas decreased with increasing Ni fraction (Table 1).

Table 1: Physicochemical properties of MA-*x*Ni and 1 wt% Ru/MA-*x*Ni.

Sample[a]	S_{BET} [$m^2 g^{-1}$]	Ni(200) crystallite size [nm][b]
MA-0Ni	348	–
1 wt% Ru/MA-0Ni	364	–
MA-10Ni	354	–
1 wt% Ru/MA-10Ni	342	–
MA-20Ni	350	–
1 wt% Ru/MA-20Ni	347	4.5
MA-33Ni	185	–
1 wt% Ru/MA-33Ni	250	5.9
MA-40Ni	176	–
1 wt% Ru/MA-40Ni	259	6.0
MA-50Ni	154	–
1 wt% Ru/MA-50Ni	188	5.5

[a] 1 wt% Ru/MA-xNi samples were prepared by conventional impregnation and reduced at 400 °C with H_2. [b] The sizes were calculated from the peak width at $2\theta = 52°$ in the XRD patterns.

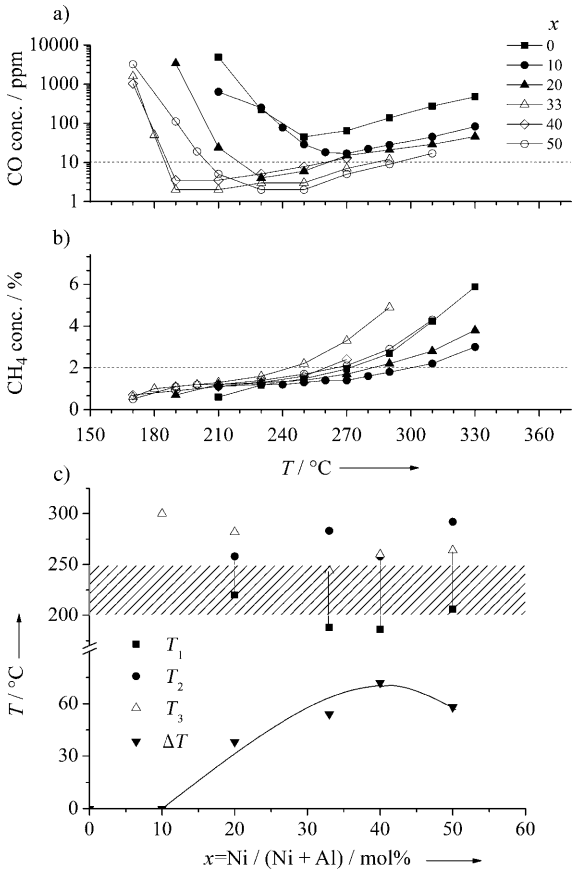

Figure 1. Temperature dependence of a) CO and b) CH_4 outlet concentrations over 1 wt% Ru/MA-*x*Ni ($x = 0$–50) for CO methanation, and c) the relationship between Ni fraction and temperature.

MA-*x*Ni impregnated with 1 wt% Ru, denoted as 1 wt% Ru/MA-*x*Ni, was prepared by conventional impregnation, followed by reduction with hydrogen at 400 °C. The catalytic activities for selective CO methanation were investigated with a fixed-bed quartz tubular reactor at atmospheric pressure. High levels of CO (1 vol%) and 20% CO_2 were fed, matching the upstream conditions in a practical reformer. The temperature dependence of CO and CH_4 outlet concentrations over these catalysts are shown in Figure 1. On every catalyst examined, the CO outlet level decreased with increasing temperature and exhibited a minimum (Figure 1a). It is obvious that the CO reduction temperature is lowered with increasing Ni content up to 40%, resulting in the reduction of CO levels to less than 10 ppm from 1 vol% for Ni contents larger than 20%, and in particular lower than 3 ppm in the cases of 33% and 40% at low reaction temperatures. It is also noteworthy that the CH_4 levels were nearly constant (less than 2%) under these lowered CO level conditions (Figure 1b). After the appearance of the minima in the CO levels, the levels increased with increasing temperature owing to the occurrence of the RWGS and also methanation of CO_2. This is a clear demonstration of the superior selectivity and high reactivity of the newly developed catalysts for the methanation of CO compared with commercial and reported catalysts (Supporting Information, Figure S3).

As shown above, it is difficult to compare the catalytic performances for CO methanation, because not only the CO conversion and selectivity but also the reaction temperature is an important parameter for practical applications. A set of three distinct temperatures was used to describe the catalytic performances for these catalysts comprehensively. First, T_1 and T_2 define the temperature range in which CO conversion is higher than 99.9%; that is, CO concentration is lower than 10 ppm, as a benchmark of conversion activity of the investigated catalysts. Second, T_3 was chosen as a threshold below which CH_4 formation was suppressed to less than 2%, indicating a selectivity for CO methanation of greater than 50%. Third, the difference between either T_2 or T_3 (whichever was lower) and T_1 was considered to be the working temperature window ΔT. Considering practical applications, ΔT should be as large as possible, preferably covering the 200–250 °C range, which is the typical working range of conventional upstream low-temperature shift reactors. Figure 1c compares the catalytic performances of the investigated materials by plotting ΔT versus the Ni mole percent *x*. T_1, T_2, and T_3 are shown to make clear the corresponding reaction temperatures. Similar to the dependence of each T value on x, ΔT is also strongly dependent on x, exceeding 50 °C and covering the temperature range of 200–250 °C for $x \geq 33\%$ and exhibiting a maximum value at 72 °C when $x = 40\%$.

It is also of great importance to confirm the long-term stability of the new catalysts for longer operation times. A durability test was carried out over 1 wt% Ru/MA-40Ni at 200 °C under the standard reaction conditions. Figure 2 shows the time courses of the changes in the CO and CH_4 outlet

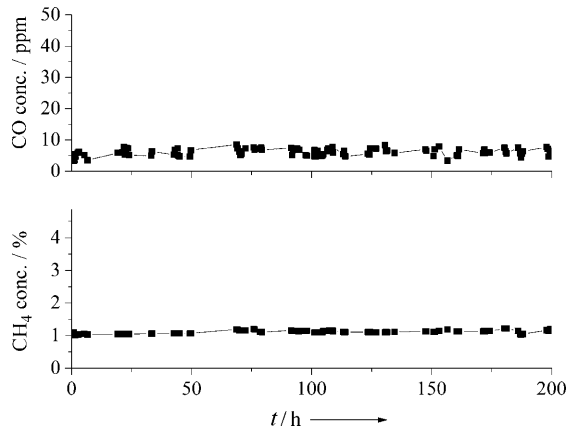

Figure 2. Durability test for CO selective methanation over 1 wt% Ru/MA-40Ni at 200 °C.

concentrations. It is clear that CO levels of less than 10 ppm were maintained for 200 h with a nearly constant CH_4 concentration of 1.1%, which means that only about 0.1% CO_2 was converted into methane. To the best of our knowledge, this is the first time that catalysts have been reported that meet the requirements for high purity hydrogen, starting from the high concentration of 1% CO in the inlet gas and reaching levels below 10 ppm with such long-term stability under standard reaction conditions. Furthermore, the catalyst preparation did not require complicated processing but instead was rather facile.

The surface areas of the 1 wt% Ru/MA-xNi catalysts after reduction at 400 °C are listed in the second column of Table 1. The samples with $x \leq 20\%$ all had very similar high surface areas, regardless of the ruthenium impregnation, whereas the catalysts with $x \geq 33\%$ without ruthenium impregnation tended to decrease in the surface area with increasing x; approximately half the surface area of the former, which might be brought by an increase of the mean mesopore size or an suppression of the formation of mesopore structure at such high nickel oxide contents. However, those catalysts showed rather increased surface areas with the impregnation of ruthenium, especially for $x = 33$ and 40. In general, the surface area should decrease to some extent after loading metal particles into mesoporous materials, if there is pore-filling. But in the present case, only 1 wt% Ru was loaded, which should not seriously affect the surface area of 1wt% Ru/MA-*x*Ni. Therefore, the increase after ruthenium impregnation must be brought about by other factors. In this system, Ni-Al mixed oxides with mesoporous structure were employed as the support to load 1 wt% Ru. During the reduction process, along with Ru^{3+} ions, some of the NiO can also be reduced, and the reduced amount of NiO will be increased owing to spill-over hydrogen from reduced Ru^0 metal sites, which enhanced the catalytic performance dramatically (Supporting Information, Figure S3).[21] The increased number of nickel particles may contribute to the increased surface areas for the 1 wt% Ru/MA-*x*Ni ($x \geq 30$) catalysts. It is likely that the structure of the resulting samples was changed from that of the original MA-xNi, particularly with a high nickel content.

The morphology of the 1wt% Ru/MA-xNi catalysts was therefore examined after H_2 reduction at 400 °C by transmission electron microscopy (TEM). Figure 3a–c shows

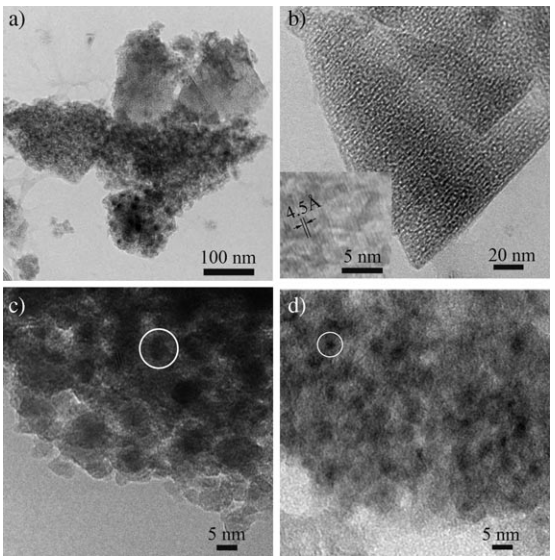

Figure 3. TEM images of a–c) 1 wt% Ru/MA-40Ni and d) 1 wt% Ru/MA-20Ni after H_2 reduction at 400 °C. Inset in Figure 3b): high-resolution TEM image.

representative TEM images of 1 wt% Ru/MA-40Ni. Two types of structures, namely black-speckled parts and triangle-like blocks were observed (Figure 3a). It is interesting to note that triangular blocks show a worm- like mesoporous structure (Figure 3b). The crystal lattice structure and pores can be observed clearly from the high-resolution TEM image (inset in Figure 3b). The triangular structure became more and regular with decreasing nickel content. From the SEM image, regular tetrahedral-shaped blocks can be observed directly (Supporting Information, Figure S4). The typical electron diffraction pattern indicates the single-crystalline structure of γ-Al_2O_3. Figure 3c shows an enlarged TEM image of black-speckled parts, which is associated with nickel, as indicated by the element mapping analysis (Supporting Information, Figure S5). It can be clearly seen that the size of black particles (marked by the white circle) was influenced by nickel content, which become smaller when x was decreased to 20 (Figure 3d). It is proposed that part of the aluminum oxide became segregated from the Ni-Al oxides, became hydrated in water during the conventional impregnation process, and formed a hydroxide. Stable γ-Al_2O_3 was then obtained after removal of water. However, the formation mechanism of the tetrahedrally shaped γ-Al_2O_3 with a worm-like mesostructure remains a mystery. As mentioned above, there was no uniform mesostructure formed for MA-*x*Ni when $x \geq 33$ induced by the low surface area, whereas after impregnation of $RuCl_3$, the formation of tetrahedral blocks make the surface area of the catalysts increase, especially when $x = 33$ and 40.

The existence of γ-Al_2O_3 in 1 wt% Ru/MA-*x*Ni after reduction by H_2 at 400 °C when $x \leq 40$ was also confirmed by

XRD patterns (Supporting Information, Figure S6). The peaks at 2θ=37, 39, 46, and 67° assigned to γ-Al_2O_3 (JCPDS 10-0425) appear on curves a–e, whereas only those assigned to NiO remain in the 1 wt% Ru/MA-50Ni sample (curve f), which began to appear when $x \geq 33$. This result indicates that only part of the NiO was reduced to the metallic state and became supported on the remaining Ni-Al mixed oxides. The nickel crystallite sizes calculated from the peak at 2θ=52° are listed in the third column of Table 1. The crystallite nickel size increased to 6 nm when $x = 33$ and 40 and then decreased with continued increase of nickel fraction. It was reported that nickel metal particles are active sites for CO selective methanation in Ru/Ni-Al mixed oxide systems.[21] In the present research, the catalysts with $x = 33$ and 40 exhibited higher catalytic performance for selective CO methanation. It is proposed that the size of the active site, particularly in black-speckled areas formed specifically by leaching out of aluminum oxide from mesoporous Ni-Al mixed oxides, plays an important role for CO selective methanation. Nickel crystallites of relatively large sizes were suitable for CO methanation. Similar results were reported by Takenka et al. and Meerten et al.[19,23]

In summary, we have successfully demonstrated that members of a series of mesoporous Ni-Al oxides with high surface areas, doped with 1 wt% Ru through a conventional impregnation process, show excellent catalytic performance for selective CO methanation in the presence of excess CO_2. The working temperature windows, in which CO was removed to less than 10 ppm from 1 vol%, with greater than 50% selectivity for CO methanation, were wider than 50 °C and covered the temperature range of 200 to 250 °C. Furthermore, long-term stability (200 h) was demonstrated, with no detectable change in the outlet CO as well as CH_4 concentrations. The facile synthesis of the catalysts with a wide range of Ni/Al ratios makes them promising catalysts for practical applications.

Experimental Section

Mesoporous Ni-Al oxides, MA-*x*Ni, with different Ni mole fractions, were prepared following the procedure described by Morris et al. by employing a triblock copolymer (Pluronic P123, BASF) as a template.[22] The resulting sample was calcined at 400 °C with a heating rate of 1 °C min^{-1} and held for 4 h. 1 wt% Ru was doped into MA-*x*Ni by conventional impregnation with an aqueous solution of $RuCl_3 \cdot n H_2O$. After drying at 110 °C for 12 h, the sample was reduced with H_2 at 400 °C.

The BET specific surface areas of the samples were determined by adsorption–desorption of nitrogen using an N_2 physisorption apparatus (Bel Japan BEL-mini). Before measurement, each sample was pretreated at 300 °C for 1 h. The X-ray powder diffraction of the samples was carried out with a Rigaku Rint-TTR2100 X-ray diffractometer (voltage 50 kV; current 300 mA) and a Rigaku Ultima IV. Scanning transmission electron microscopy (STEM) images and TEM images were observed on a Hitachi HD-2300 and Hitachi H-9500 electron microscope, respectively.

The catalytic activity tests were performed with a fixed-bed quartz tubular reactor at atmospheric pressure. The catalyst powder was shaped and sieved into pellets with diameters of 1.2–2.0 mm. The volume of each catalyst used for activity test is 2.8 mL. Before reaction, the catalyst was pretreated at 400 °C with H_2 for 1 h. The feed gas of 1 vol% CO and 20 vol% CO_2 with H_2 making up the balance was mixed with a mass-flow controller. The gas hourly space velocity (GHSV) was adjusted to 2400 h^{-1} on a dry basis. Steam (15%) was added into the mixed gas supplied by an HPLC pump (AT-220, Att Mol Inc.) through a vaporizer. The reaction temperatures were measured with thermocouples above and below the catalyst layer. An on-line gas chromatograph with a thermal conductivity detector (TCD, GC-390B, GL Sciences, Inc.) was used to analyze the inlet and outlet gas composition. A molecular sieve (13X) column was used for the separation of methane and carbon monoxide, and a Porapak Q column was used for carbon dioxide. Furthermore, a flame ionization detector was employed to detect CO at lower levels (ppm), where CO was separated by a molecular sieve column and then converted into methane in a methanizer.

Received: September 9, 2010
Revised: October 5, 2010
Published online: November 29, 2010

Keywords: fuel cells · hydrogen · mesoporous oxides · methanation · ruthenium

[1] S. Gottesfeld, US 4,910,099, **1990**.
[2] R. A. Lemons, *J. Power Sources* **1990**, *29*, 93.
[3] J. J. Baschuk, X. Li, *Int. J. Energy Res.* **2001**, *25*, 695.
[4] L. P. L. Carrette, K. A. Friedrich, M. Huber, U. Stimming, *Phys. Chem. Chem. Phys.* **2001**, *3*, 320.
[5] A. N. J. van Keulen, J. G. Reinkingh, US 6,403,049 B1, **2002**.
[6] N. Edwards, S. R. Ellis, J. C. Frost, S. E. Golunski, A. N. J. van Keulen, N. G. Lindewald, J. G. Reinkingh, *J. Power Sources* **1998**, *71*, 123.
[7] M. Watanabe, H. Uchida, H. Igarashi, M. Suzuki, *Chem. Lett.* **1995**, 21; M. Watanabe, JP Patent, JP 07256112, **1995**, US Patent, US 6,168,772, **2001**.
[8] H. Igarashi, H. Uchida, M. Suziki, Y. Sasaki, M. Watanabe, *Appl. Catal. A* **1997**, *159*, 159; H. Igarashi, H. Uchida, M. Watanabe, *Chem. Lett.* **2000**, 1262; H. Igarashi, H. Uchida, M. Watanabe, *Stud. Surf. Catal.* **2001**, *132*, 953.
[9] M. Watanabe, H. Uchida, K. Ohkubo, H. Igarashi, *Appl. Catal. B* **2003**, *46*, 595.
[10] a) M. Kotobuki, A. Watanabe, H. Uchida, H. Yamashita, M. Watanabe, *J. Catal.* **2005**, *236*, 262; b) M. Kotobuki, A. Watanabe, H. Uchida, H. Yamashita, M. Watanabe, *Appl. Catal. A* **2006**, *307*, 275; c) N. Maeda, T. Matsushima, H. Uchida, H. Yamashita, M. Watanabe, *Appl. Catal. A* **2008**, *341*, 93.
[11] W. Wang, Y. Chen, *Appl. Catal.* **1991**, *77*, 21.
[12] K. B. Kester, E. Zagli, J. L. Falconer, *Appl. Catal.* **1986**, *22*, 311.
[13] N. W. Gupta, V. S. Kamble, K. A. Rao, R. M. Iyer, *J. Catal.* **1979**, *60*, 57.
[14] Y. Borodko, G. A. Somorjai, *Appl. Catal. A* **1999**, *186*, 355.
[15] B. S. Baker, J. Buebler, H. R. Linden, J. Meek, US Patent, 3,615,164, **1968**.
[16] A. Rehmat, S. S. Randhava, *Ind. Eng. Chem. Prod. Res. Dev.* **1970**, *9*, 512.
[17] S. I. Fujita, N. Takezawa, *Chem. Eng. J.* **1997**, *68*, 63.
[18] Z. Zhang, G. Xu, *Catal. Commun.* **2007**, *8*, 1953.
[19] S. Takenaka, T. Shimizu, K. Otsuka, *Int. J. Hydrogen Energy* **2004**, *29*, 1065.
[20] R. A. Fagle, Y. Wang, G. Xia, J. J. Strohm, J. Holladay, D. R. Palo, *Appl. Catal. A* **2007**, *326*, 213.
[21] M. Kimura, T. Miyao, S. Komori, A. Chen, K. Higashiyama, H. Yamashita, M. Watanabe, *Appl. Catal. A* **2010**, *379*, 182.
[22] S. M. Morris, T. F. Fulvio, M. Jaroniec, *J. Am. Chem. Soc.* **2008**, *130*, 15210.
[23] R. Z. C. van Meerten, A. H. G. M. Beaumont, P. F. M. T. van Nisselrooij, J. W. E. Coenen, *Surf. Sci.* **1983**, *135*, 565.

